RESEARCH ARTICLE

Improving the thermostability of GH11 xylanase XynXM from *Aspergillus brunneoviolaceus* CBS 621.78 by the design of cord region

Tongbiao Li[1], Jiaze Tang[2], Siqi Li[1], Hui Peng[1], YanYan Zhu[1], Jinjin Zhu[1], Yue Li[1], Chaoying Liu[1], Enzhong Li[1, *]

[1]School of Biological Science and Food Engineering, Huanghuai University, Zhumadian 463000, Henan, China. [2]School of life sciences, Xinyang Normal University, Xinyang 464000, Henan, China

Xylanases which hydrolyze β-1,4-glycosidic bonds of xylans to yield xylooligosaccharides have a potential to be used in pulp bleaching, food processing, and feed processing. However, the poor thermostability of xylanases is a critical limiting factor in industrial applications. The thermostability of xylanases can be improved by protein engineering and computer-assisted design. In the present study, the thermostabilizing mutation G143W locating at the cord region of xylanase XynXM from *Aspergillus brunneoviolaceus* CBS 621.78 was predicted by the FireProt web server and constructed by site-directed mutagenesis. Heat tolerance experiments were performed in mutant G143W and wildtype XynXM. G143W exhibited a substantially improved thermostability with half-life of inactivation at 45℃ enhanced from 41.5 min to 65.3 min, which was approximately 1.6-fold increase over that of wildtype. Furthermore, the optimum temperature was 50℃, which has the best reactive activity, and 5℃ higher than that of XynXM (45℃). The reactive optimal pH of G143W increased from pH 5.0 to pH7.0. The pH stability span (4.0-9.0) of G143W displayed a significant improvement comparing to that of XynXM. Comparing to the wildtype, the half-life of G143W at 35℃ in simulated intestinal fluid (pH 6.8, 10 mg/mL trypsin solution) was increased by 35.8 min. Novel hydrophobic contacts and hydrogen bonds were discovered in the model of G143W, which explained the reason of enhanced thermal stability. The key residues Trp57, Asn84, Val86, Tyr114, Gln117, Trp120, Glu127, Tyr137, Pro139, Ser141, Thr144, Ala161, Pro167, and Glu218 were identified in protein-ligand interaction by the molecular docking analysis using AutoDock Vina, which contributed to the catalytic activity and stability of enzyme. This study developed a thermostabilizing mutant G143W locating in the cord region of xylanase by the prediction of FireProt web server, which laid a foundation for exploring the functional relationship between cord region and xylanase XynXM.

Introduction

As a heterogeneous polysaccharide, xylan is made mainly from β-1,4-glycoside bonds linking xylose and arabinose, which is an important component of plant hemicellulose, accounting for about 15% ~ 35% of the dry weight of plant cells [1, 2]. As group of glycoside hydrolases (GH), xylanases can hydrolyze the-1,4-glycoside bond of xylan and generate functional xylo-oligosaccharides [3, 4]. Based on the differences of structure, catalytic mechanism, and physical and chemical properties, xylanases can be divided into 5, 7, 8, 10, 11, and 43 families of glycoside hydrolases, mainly GH10 and GH11 families [5]. Comparing to GH10 xylanases, GH11

xylanases are attracting more attentions due to their strict substrate selectivity, simple structure, high catalytic efficiency, and wide ranges of temperature and pH optima [6, 7]. In nature, the source of GH11 xylanases is very extensive, which can be obtained from lots of microorganisms, such as actinomycetes, fungi, and bacteria [8]. Meanwhile, as a crucial biocatalyst, xylanases are widely used in pulp bleaching, food processing, feed processing, textile, and brewing [9, 10]. For example, in the feed processing, xylanases can decompose non-starch polysaccharides (NSPS) into oligosaccharides with less polymerization, eliminate and reduce the anti-nutritional effect of non-starch polysaccharides gave rise to by large viscosity in the animal stomach, thus improving the performance of feed [11-13].

As an important feed enzyme, the thermal stability of xylanases is the essential condition in the industrial application [14, 15]. In the industrial process, heat-resistant xylanases can effectively reduce the load of enzyme and achieve high production efficiency [16, 17]. However, most natural and highly active xylanases belong to mesophile xylanase with poor thermal stability, making them a critical limiting factor in industrial applications [18-20]. Therefore, how to improve the thermostability of xylanases has always been a critical problem to be solved by researchers. In view of this problem, many researchers have carried out in-depth research. Fruitful work has been carried out around the main secondary structural components of GH11 xylanases, β-folding and α-helix structures [21-24]. A large number of studies have found that factors such as hydrophobic interactions, disulfide bonds, salt bridges, hydrogen bonds, and amino acid ratios in these secondary structures have significant effects on the thermal stability of xylanases [25, 26]. Recent studies have revealed that reducing the enzyme's flexibility and reinforcing the enzyme's rigidity are beneficial to improve its thermal stability [27-29]. The cord serves as the main assembly in the GH11 xylanases, belonging to the loop region, which displays high flexibility and influents the stability of enzymes [30].

Therefore, how to enhance the rigidity of cord to stabilize the protein structure and obtain thermal stability xylanases has becomes a new strategy and excited great interest among researchers. To explored effect of the cord region on the thermal stability of GH11 xylanases, computer-aided design and structural alignment were performed by Li, *et al*. [21]. The cord region (93GTYRPTG99) of GH11 xylanase AoXyn11A from *Aspergillus oryzae* CICC40186 was substituted by the cord region (93GTYNPGSGG101) of xylanase PXYL11 from *Thermobifida Fusca* to construct the mutant ATX11A41/CORD. The optimum temperature of mutant ATX11A41/CORD was 65℃, which was 15℃ higher than that of Wildtype AOXYN11A. This study showed that the cord region of GH11 xylanases might play a crucial role in improving the thermal stability. Numerous studies showed that a number of in silico tools were available and effective for designing the thermostable mutants of enzymes [31-33]. A growing number of xylanases have been engineered to improve heat resistance by in silico strategy [34, 35].

The FireProt is a recently developed web server, which combined energy- and evolution-based strategies, used three enzyme engineering strategies and sixteen protein structure computational tools for rapid and effective design of thermal stability of protein, and could design single-point mutants as well as predict multiple-point mutants with rational recombinant strategy of single-point variants [36].

For the purpose to explore the effect of the cord region of GH11 xylanase XynXM (GenBank accession number: XM_025588189.1) from *Aspergillus brunneoviolaceus* CBS 621.78 on the thermostability, the key residue of cord region was identified by using the FireProt web server. The potentially thermostable mutant was constructed by site-directed mutagenesis. The results from this study may lay a foundation for exploring the functional relationship between cord region and xylanase XynXM and provide new insights in engineering a thermostable xylanase.

Materials and methods

Homology modeling and docking of the recombinant xylanases

The amino acid sequence of recombinant xylanase XynXM (GenBank accession number: XP_025442333.1) was submitted to SWISS-MODEL (https://swissmodel.expasy.org/) for homology modeling. The model was further optimized and evaluated with the Discovery Studio 3.0 (https://discover.3ds.com/discovery-studio-visualizer-download), while dihedral angles by Ramanchandran Plot, amino acid matching degree by Profile-3D, and the model optimization and evaluation steps were performed with default procedures [37]. The effects of mutant G143W on protein stability were anatomized by using the PIC server (http://pic.mbu.iisc.ernet.in/job.html) and the DynaMut (http://biosig.unimelb.edu.au/dynamut/) with the default parameters [38]. By using the three-dimensional structure of recombinant xylanase as the receptor, the substrate xylose was docked to a suitable location in the active pocket of enzyme using the AutoDock 4.2 program (Olson, San Diego, California, USA) [39]. Electrostatic potentials of the wildtype enzyme (XynXM) and mutant were calculated by Adaptive Poission-Bolzmann Solver (APBS) (https://www.poissonboltzmann.org/) [40]. The structure of xylanase was visualized and analyzed with PyMOL (Schrödinger, New York, NY, USA).

Site-directed mutagenesis

The mutated G143W was constructed by Fast site-Directed Mutagenesis System according to the manufacturer's instructions (Vazyme, Nanjing, Jiangsu, China). Polymerase chain reaction (PCR) amplification was performed by using forward primer G143W-F (5'-AAC CCC GGC TCA GCT TGG ACT TAC AAA GGC TCG-3') and reverse primer G143W-R (5'-CGA GCC TTT GTA AGT CCA AGC TGA GCC GGG GTT-3'). The PCR reaction mixture include 2× Max Buffer (25 μL), 2 μL of forward primer (10 mM), 2 μL of reverse primer (10 mM), 1 μL of dNTP Mix (10 mM), 1 μL of template DNA (20 ng/μL), 1 μL of Phanta Max

Super-Fidelity DNA Polymerase, and then ddH$_2$O to a total volume of 50 μL. The PCR cycling conditions consisted of an initial step of 3 min at 98℃, followed by 25 cycles of denaturation at 98°C for 30 s, annealing at 55℃ for 45 s, and elongation at 72°C for 2 min, and an extra elongation at 72℃ for 10 min. The PCR products were digested by using the restriction enzyme Dpn I (New England Biolabs, Ipswich, MA, USA) at 37℃ for 30 min, then transformed into *E. coli* DH5α competent cells. The positive clones were screened on Luria-Bertani (LB) medium plates containing 50 ug/mL of Kanamycin (Sangon Biotech Co., Ltd, Shanghai, China) and incubating at 37℃ overnight. DNA sequencing was performed to verify the mutants by Sangon Biotech Co., Ltd. (Shanghai, China).

Protein expression and purification

The recombinant plasmids, pET-28a-XynXM and pET-28a-G143W, were transformed into *E. coli* BL21 for the expression of xylanases. The transformants were inoculated in 2 mL of LB medium containing Kanamycin and incubated at 37℃ with the shaking speed of 180 rpm, overnight. Afterward, 1 mL of the culture suspension was transferred into fresh 100 mL of LB medium containing Kanamycin and incubated again at 37℃ with the shaking speed of 180 rpm until optical density (OD$_{600}$) reached 0.6-0.8. After that, 2 mM of isopropyl β-d-1-thiogalactopyranoside (IPTG) was added into the culture suspension and incubated at 30℃ for 2 h for protein expression. The cells were harvested by centrifugation at 6,000 rpm for 10 min at 4 ℃ and resuspended the pellet with sodium dihydrogen phosphate-citrate buffer (pH 6.0). To obtain the crude enzyme solution of recombinant xylanases, supernatants were harvested after the cells were disrupted by sonication and centrifugation at 1,2000 rpm for 20 min at 4℃. The recombinant xylanases were purified by using Ni-NTA Sefinose^{TM} Resin Kit (Sangon Biotech, Shanghai, China) according to the manufacturer's instructions. The protein was equilibrated with binding buffer containing 10 mM imidazole, and then, was eluted by elution buffer supplemented with 250 mM imidazole,

and finally was dialyzed against the same buffer without containing imidazole. The purified protein was checked by SDS-PAGE method, and the concentration of enzyme was determined by Bradford protein assay kit (Sangon Biotech Co., Ltd, Shanghai, China).

Enzyme assays
Based on the 3,5-dinitrosalicylicacid (DNS) method, the activities of recombinant xylanases were calculated by measuring the release of reducing sugars (xylose) hydrolyzed from beechwood xylan [12]. The reaction mixture contained 1.5 mL of 0.5% beech xylan and 1 mL of properly diluted enzyme solution. The reaction was set for 15 min at appropriate temperature, and then, was terminated by adding 2.5 mL of DNS solution, boiled for 7 min. 5 mL of ddH$_2$O was added to the reaction after cooling down, and the absorbance value was measured at 540 nm. The enzyme activity of xylanase was defined as 1 active unit (U) of the enzyme equaled to the amount of enzyme needed to hydrolyze xylan to generate 1 µmol of xylose per minute under the above conditions.

The temperature and pH characteristics of the wildtype XynXM and mutant G143W
The optimal temperatures of purified wildtype and mutant enzymes were examined from 35-60℃ under the conditions of enzyme activity determination method described above. Thermostability of enzymes was determined by incubating the purified xylanases without xylan at 40℃, 45℃, and 50℃ for 1h, respectively. The half-lives (t$_{1/2}$) of xylanases were calculated according to Liu, *et al*. method [41]. Analogously, the optimal pH of wildtype and mutant enzymes at pH range of 4.0-9.0 was measured under the optimal temperature, respectively. The pH stability of xylanases was determined after incubation in various buffer systems at pH 4.0-9.0 for 1 h at 40℃. The residual activity of xylanases was measured by the DNS method. All experiments were carried out in triplicate.

Resistance analysis of the recombinant xylanase to trypsin solution

The purified xylanases were mixed with the artificial intestinal fluid (pH 6.8, 10 mg/mL of trypsin solution) (Sangon Biotech Co., Ltd, Shanghai, China) in the mass ratio of 10:1, respectively. The residual activities of enzymes were determined after incubation at 35℃ for 150 min. All experiments were carried out in triplicate.

Results and discussion

Homology modeling and identification of the potential thermostabilizing mutant G143W
The initial model of XynXM was built by SWISS-MODEL, which was submitted to Discovery Studio for further optimization. The final model was shown in Figure 1a consisting of two twisted anti-parallel β-sheets and one single α-helix and resembling a typical β-jelly-roll fold structure. Glu127 and Glu218 predicted by Prosite (http://prosite.expasy.org) were the catalytic residues, which located at the side of the catalytic active pocket cleft. Based on the evaluation of Ramachandran Plot, 95.7% of amino acid residues located in the allowed region of the plot (Figure 1b). The amino acid verify score calculated by Profile-3D displayed all above the "0 line", which exhibited that the model of XynXM had a high matching degree with its amino acid sequence (Figure 1c). The above evaluation results showed that the modeling structure had high reliability and could be used for subsequent experiments.

To gain insight into the influence of cord on the thermal stability of GH11 xylanase XynXM, FireProt web server was used to calculate the key residues of thermostability in the cord regions. Fireprot web server is a very promising tool, which predicts thermal stability related sites of protein by energy- and evolution-based strategies. Energy strategy depends on the crystal structure information of protein, while the evolution strategy is based on the evolutionary information of amino acid sequence [31]. The most important feature of FireProt web server is able to predict multi-site mutants,
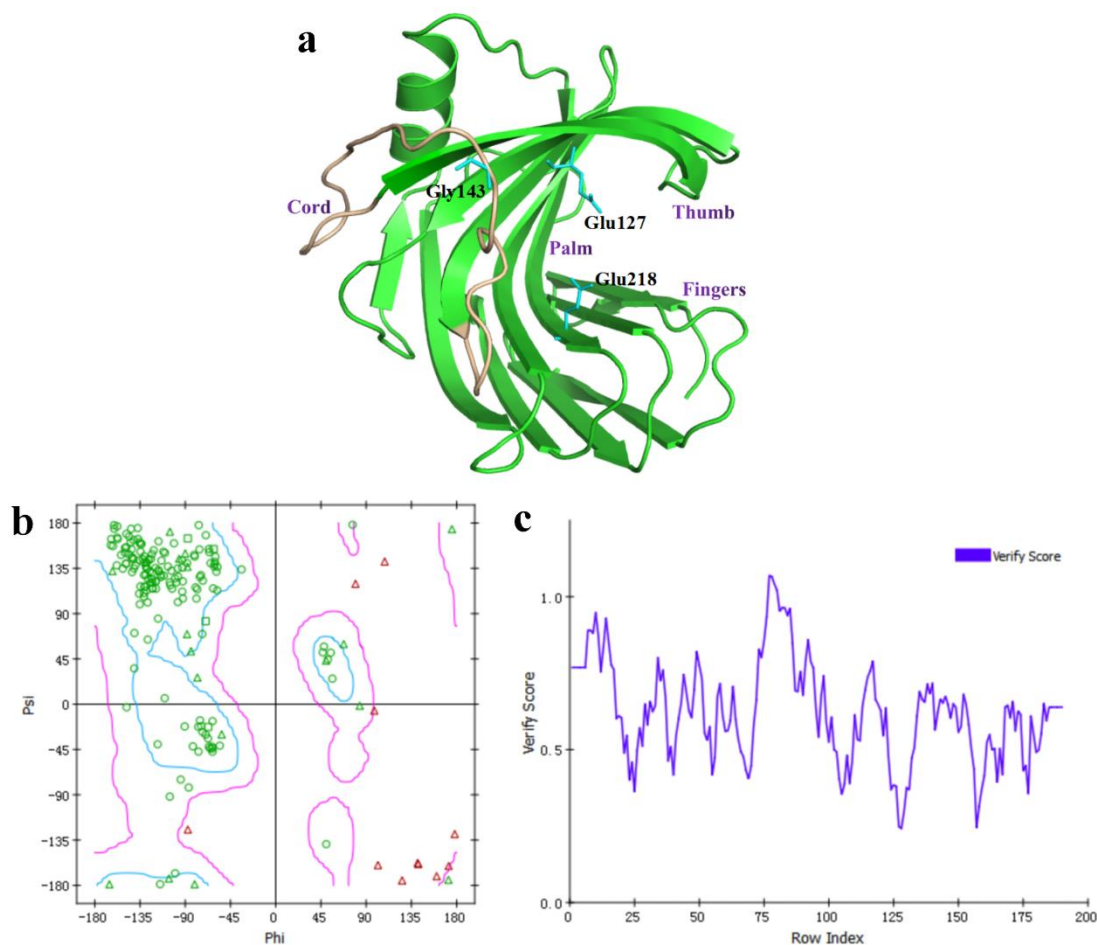
Figure 1. The structural model of XynXM (a), the evaluation of Ramachandran Plot (b), and the evaluation of Profile-3D (c). Cayn sticks showed the predicted Gly143, the catalytic residues Glu127, and Glu218, respectively.

eliminates some conservative and highly correlated amino acid sites, filters some potential deleterious mutations and superpose single-site mutants, thus designs the multi-site mutants in one step [42]. In fact, FoldX and Rosetta used by FireProt to calculate the free energy of mutation are able to predict the thermal stability mutant, and the algorithm focuses on the local stability of protein [12]. Based on the final model of XynXM, the thermostabilizing related sites of XynXM were predicted by the FirePort web server. Seventeen mutant sites were obtained, respectively (Table 1). Among them, the virtual mutant G143W locating at the cord region had the lowest folding free energy ($\Delta\Delta G_{fold}$), which was computed by using FoldX, by subtracting the change in the folding free energy of the wildtype (ΔG_{fold}) from the change in the folding free energy

of the mutant (ΔG_{fold}). According to the principle that the lower the energy, the more stable the structure [36], and based on the change of folding free energy after protein mutation, the mutant G413W was supposed to contribute significantly to the improvement of thermal stability.

Construction and characterization of the recombinant xylanases
The mutant G143W displayed the similar molecular mass (~28 kDa) to the wildtype by the analysis of SDS-PAGE and purified to electrophoretic homogeneity (Figure 2). The optimal temperature of the mutant G143W was 50℃, which was increased by 5℃ comparing to that of the wildtype XynXM (45℃). The result indicated that XynXM acquired a higher

Table 1. Mutations predicted by energy-based and evolution-based approach.

Chain	Mutation	Conserved	Correlated	BTC by majority	BTC by ratio	FoldX (kcal/mol)	Rosetta (kcal/mol)
Combined mutant:				-22.01 kcal/mol (17 mutations)			
B	G43P	N	N	N	Y	0.44	-
B	T58C	N	N	N	N	-1.17	-3.99
B	E66T	N	N	Y	Y	0.05	
B	S68T	N	N	Y	Y	0.01	-
B	S83W	N	N	Y	Y	-1.65	-3.52
B	N97F	N	N	N	N	-2.12	-2.04
B	D98T	N	N	N	N	-0.28	-
B	V126I	N	N	Y	Y	-0.10	-
B	E136T	N	N	Y	N	0.16	-
B	A142G	N	N	Y	N	-0.14	
B	G143W	N	N	N	N	-2.63	-6.26
B	S148T	N	N	Y	N	-0.00	-
B	N157D	N	N	Y	N	0.36	-
B	T176Y	N	N	N	N	-1.09	-2.73
B	T184S	N	N	N	Y	0.25	-
B	A201L	N	N	N	N	-1.10	-7.32
B	N211F	N	N	N	N	-1.03	-3.01
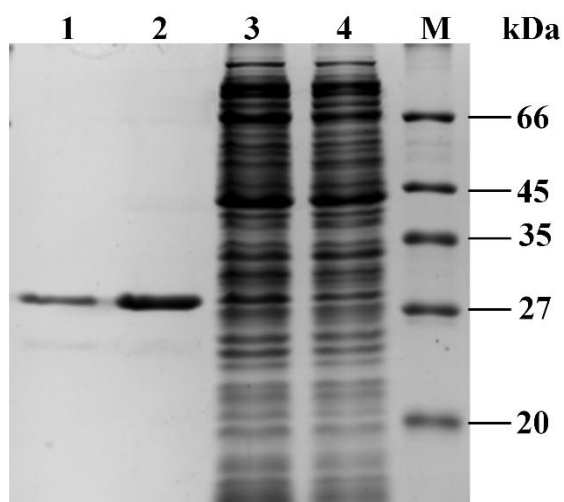
Figure 2. SDS-PAGE analysis of the wildtype XynXM and mutant G143W. **M:** protein marker. **Lane 1:** the purified G143W. **Lane 2:** the purified wildtype XynXM. **Lane 3:** the crude wildtype XynXM. **Lane 4:** the crude G143W.

temperature adaptability after mutation from Gly143 to Trp143 at the cord region (Figure 3a). To determine the thermal stability of xylanases, the residual activities of the enzymes were tested after incubation without substrate at 40℃, 45℃, and 50℃ for 1 h, respectively (Figure 3b). It was

found that the mutant G143W displayed greater heat resistance than the wildtype XynXM. After 1 h of incubation at 40℃, G143W was able to retain approximately 80% activity, while the wildtype decreased obviously and remained 64.2% of activity. In addition, G143W retained more than 60% activity after incubation for 1 h at 45℃, which was significantly higher than that of wildtype at the same conditions. Specifically, after heating treatment at 50°C for 1 h, G143W exhibited over 50% activity, which was higher than that of the wildtype (37.2%). The half-live of thermal inactivation ($t_{1/2}$) of G143W estimated at 50℃ represented an impressive result, which was enhanced from 41.5 min to 65.3 min, approximately 1.6-fold increased over that of wildtype.

After exploring thermostability of the mutant G143W, the effects of various pH (from 4.0 to 9.0) on G143W activity were checked (Figure 3c, 3d). Comparing to the wildtype, the optimal pH of G143W showed a significant increase from pH 5.0 to pH 7.0, which indicated that the activities of G143W were more suitable for the neutral pH and more than 50% of activity was observed at
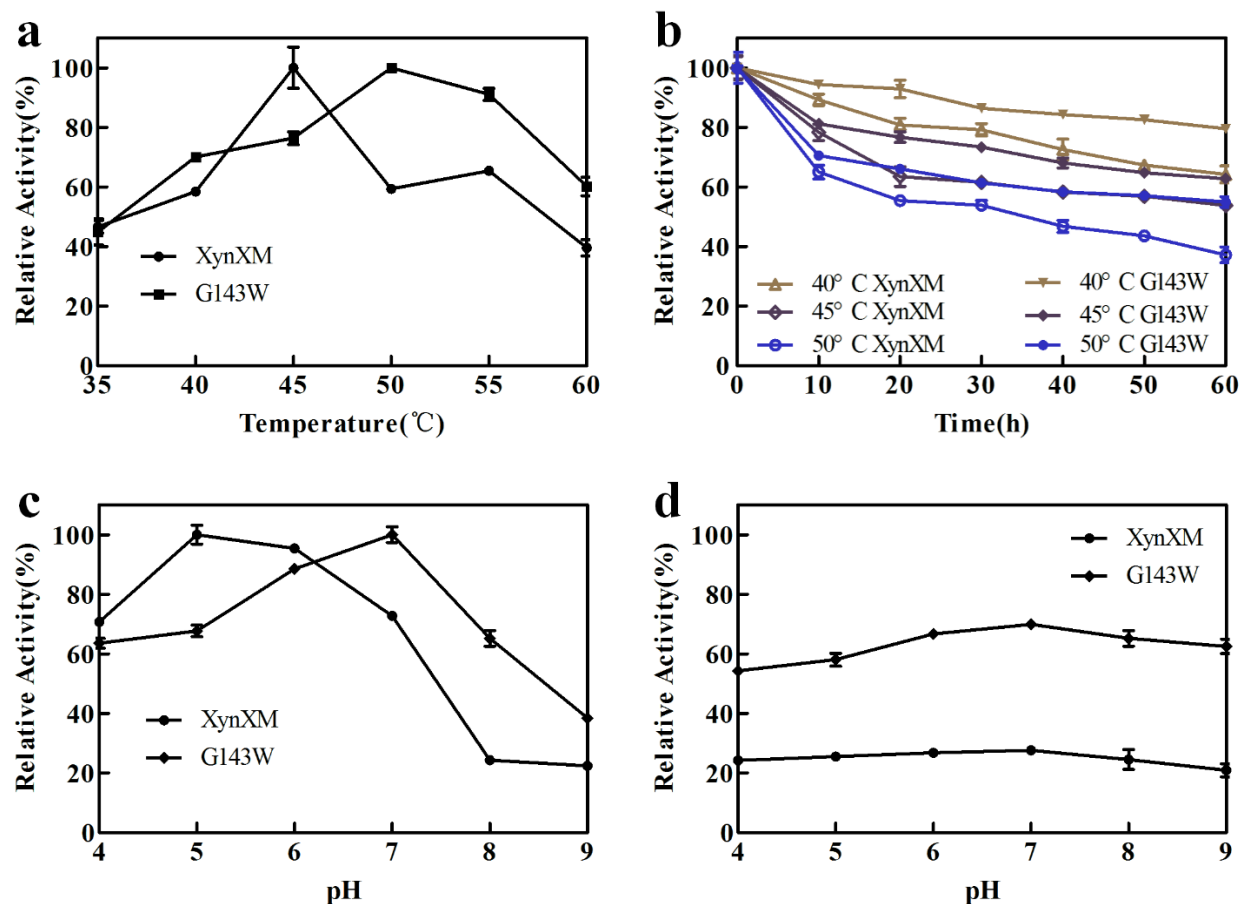
Figure 3. Optimal temperature (a) and thermostability (b), optimal pH on the activity (c) and pH stability (d) of the wildtype XynXM and mutant G143W.

pH range between 4.0 and 8.0. According to the pH stability assays, G143W showed the significant improvement after incubation for 1 h at 40℃, which displayed over 50% residual activities at pH 4.0-9.0. Whereas the residual activities of wildtype were distributed in 20-30% at the same pH condition. These results indicated that the mutant G143W was more pH resistance than the wildtype.

Evaluation of trypsin resistance
High quality xylanases tend to have good thermal stability, stability over a wide range of pH, and resistance to protease degradation in the stomach. The ability of xylanase to resist trypsin degradation is a vital characteristic as a feed enzyme. To explore the resistance of the wildtype XynXM and mutant G143W to trypsin,

the wildtype XynXM and mutant G143W were treated with artificial simulated intestinal fluid (mass ratio of 10:1) at 35℃ for 150 min. The residual activities of the enzymes were determined by sampling every 30 min. The results showed that the residual activities of G143W were significantly higher than that of the wildtype. As shown in Figure 4, G143W still retained 50% residual activities after treatment with 150 min. Whereas, the residual activities of wildtype were 39.1 % at the same conditions. The stability half-lives of wildtype and mutant G143W in trypsin solution were 103.6 min and 139.4 min, respectively. Comparing to the wildtype, the half-life of G143W in trypsin solution was increased by 35.8 min. The results showed that the mutation G143W could also significantly improve the resistance to trypsin.
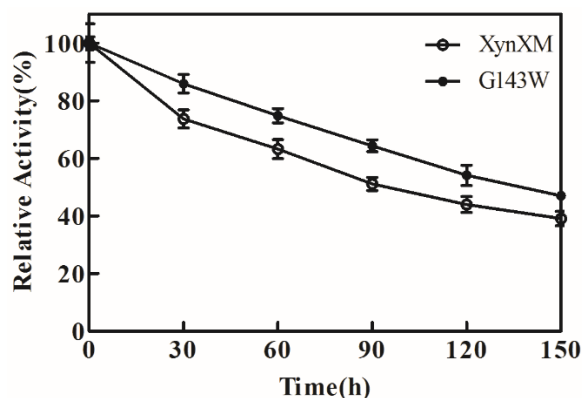
Figure 4. Effect of trypsin treatment on stability of the wildtype and mutant G143W.

Improved thermostability of the mutant G143W explored by structural simulations

To understand the thermostability mechanisms of the mutant G143W, the structural model of G143W was constructed by using the wildtype XynXM as the template. Mainly, mutations with enhanced heat resistance may be attributed to hydrogen bonds, hydrophobic contacts, stabilization of flexible loop, salt bridge, ionic interactions, and disulfide bridges. To gain insight in the increased thermostability, the intramolecular interactions of mutated residue were analyzed by the PIC server. The result indicated that the G143W mutation could form two additional hydrogen bonds with Thr160, and could add new hydrophobic interactions between Tyr145, Tyr159, and Ala161 within 5Å. The DynaMut web server, which can assess the effect of mutations on protein dynamics and stability resulting from vibrational entropy changes, revealed that the intramolecular interactions of the G143W mutation were consistent with the results predicted by PIC serve (Figure 5a and 5b). Generally, structures of thermophilic proteins often associate with higher degrees of rigidity. The flexible cord is not conducive to the stability of enzyme [43]. Additional hydrogen bonds and novel hydrophobic contacts were discovered in the mutant G143W, which can further stabilize the structure of enzyme, and increase the rigidity of cord. The beneficial site Gly143 identified by FireProt located in the cord region may also

contribute more to the overall stability. To further decipher the improvement of thermostability for the G143W mutation, electrostatic characteristic was calculated by APBS (Figure 5c and 5d). It was found that electrostatic potential of the mutated Trp143 as well as nearby local surface was light white, exhibiting fewer positive charges than that of the wildtype XynXM, which was well accepted that less positive and negative charges groups on surface played vital roles in protein stability. This result further indicated that the surface of GH11 xylanases containing less positively charged in the mutated area yielded an improvement of thermostability.

Docking analysis of wildtype and mutant G143W

The flexible cord region of GH11 xylanase is located on the side of the catalytic active pocket, which is of great significance for substrate-binding, catalysis, and stability of the enzyme. To identify the effect of G143W substitution on substrate binding, docking was performed by AutoDock 4.2 based on the predicted model. It has been reported that, in the catalytic reactions of xylanase, only a few hexacyclic xylan residues in the long chain of the substrate xylan were embedded in the active pocket, and other xylan residue chains extended out of the active pocket. During the catalytic reaction, xylan was hydrolyzed in turn into the active pocket by the structure of the xylose ring [44]. Based on the catalytic mechanism, the pentaxylose containing five xylose rings was selected as the substrate to reduce the amount of xylan calculation in the docking process (a). The docking pose with least binding affinity was selected for the analysis of enzyme-substrate interaction. Figure 6 displayed the binding conformation of xylanase with substrate pentaxylose (a). The results of docking indicated the involvement of Trp57, Asn84, Val86, Tyr114, Gln117, Trp120, Glu127, Tyr137, Pro139, Ser141, Thr144, Ala161, Pro167, and Glu218 residues in the formation of complex XynXM-pentaxylose with bond length within 5.0 Å, which was critical for protein-ligand interaction. Based on this information, mutations in the residues may increase the catalytic activity
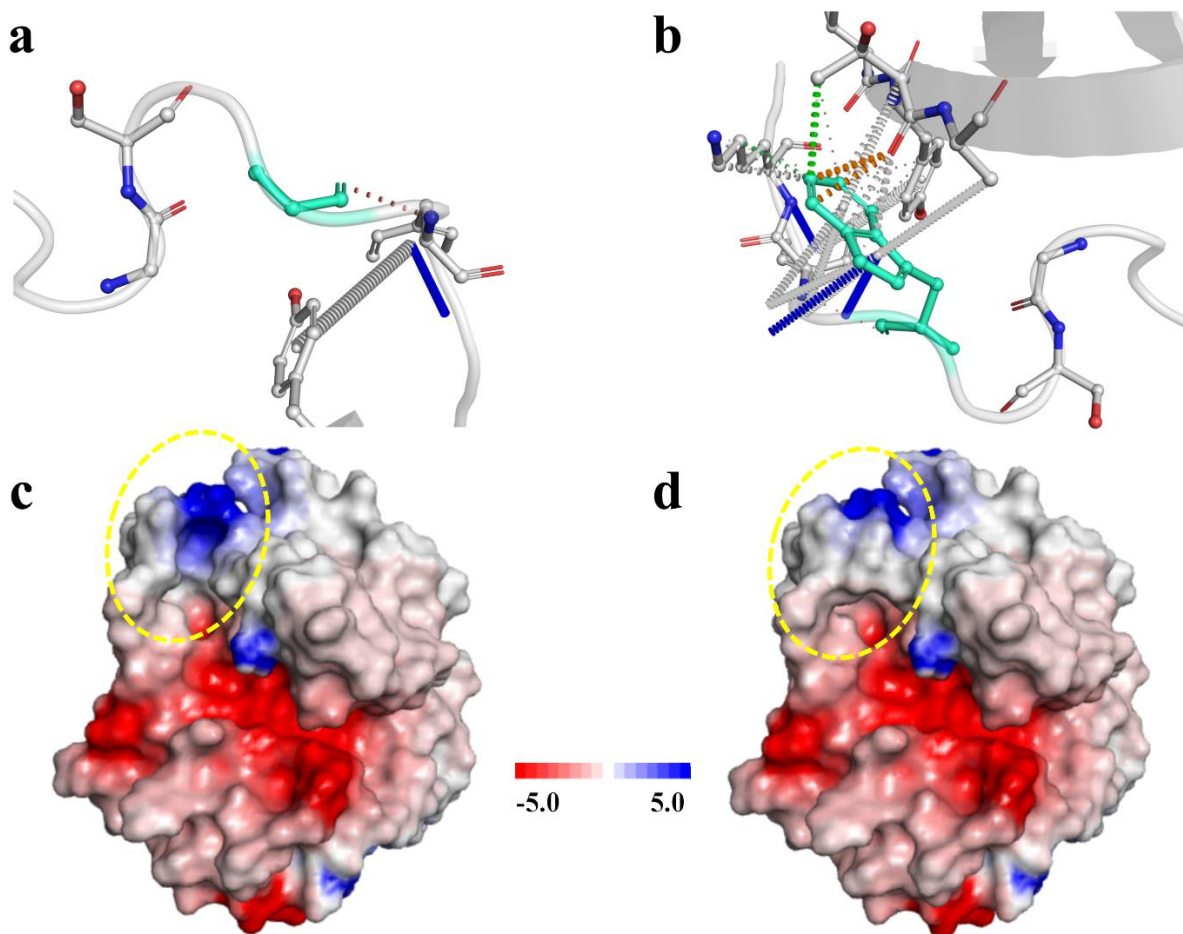
Figure 5. Intramolecular interactions of the wildtype (a) and mutant G143W (b) residues predicted by DynaMut web server. Electrostatic properties of the wildtype (c) and mutant G143W (d). The cyan stick modes showed mutated residues. The color of each interaction type was defined as follows: green, orange, blue, red, and yellow dotted line represented hydrophobic contacts, weak hydrogen bonds, halogen bonds, hydrogen bonds, respectively. Yellow dotted ring on the electrotatic potential surface represented the region of mutated sites.

and stability of enzyme. Meanwhile, it was found that a number of aromatic amino acids (Trp57, Tyr114, Trp120, Tyr137, Pro139, Pro167) were close to the substrate in the docked model, which could further stabilize the binding conformation and thermostability [45]. The identified key amino acid residues surrounding the bond substrate can contribute significantly to substrate binding, catalysis, and stability. The design of mutants around these residues may obtain the excellent properties of xylanase. In addition, in the model of wildtype XynXM docked with (a), some hydrogen bonds were formed between substrate (a) and residues Asn84, Gln117, Trp120, and Thr144, which was supposed to facilitate the binding of substrates.

Nevertheless, due to the substitution of G143W, the space of residue Gly41 was occupied by aromatic amino acid Trp143 with larger side chain, which resulted in the head of substrate not being able to bond in the space. Therefore, the orientation of the substrate rotated at a certain angle in the model of mutant G143W docked with (a) comparing to the wildtype, which enabled the formation of hydrogen bonds change significantly. In addition to the hydrogen bond between (a) and Asn84, substrate (a) formed new hydrogen bonds with Glu127, Tyr137, Arg163, and Glu218. Among new hydrogen bonds, two of them were formed with the catalytic residues (Glu127 and Glu218), and similar hydrogen bonds were not observed in the
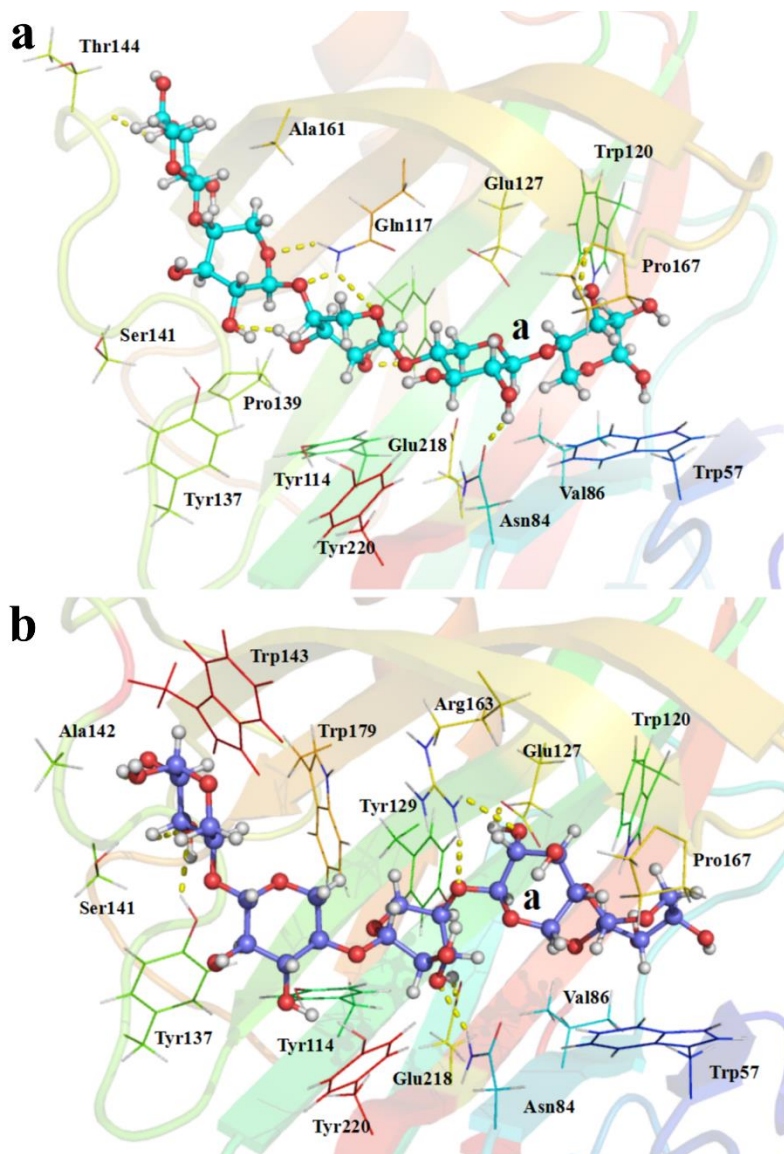
Figure 6. Docking of the wildtype XynXM (a) and mutant G143W (b) with substrate (**a**). The varied residues of wildtype XynXM and mutant G143W were shown in line. The docked substrate was shown as a ball and stick model. The hydrogen bonds were indicated as yellow dotted lines.

model of wildtype XynXM docked with (a), which would be efficient to enable the hydride transfer and improved catalytic efficiency comparing to the wildtype.

Conclusion

This study successfully identified residue Gly143 locating in the cord region of XynXM for the potential key site of thermal stability and constructed the mutant G143W. The results exhibited that G143W showed higher thermostability than that of the wildtype XynXM. The optimal temperature of G143W was 50℃, which was increased by 5℃ comparing to the wildtype XynXM. G143W displayed a substantially improved half-life at 50℃, which enhanced from 41.5 min to 65.3 min, and approximately 1.6-fold increased over that of wildtype. The pH stability assays showed that G143W also demonstrated a significant increase

in pH resistance comparing to XynXM. This study demonstrated that the G143W locating in the cord region was crucial to the thermostability of XynXM. Trypsin resistance experiments displayed that the half-life of G143W at 35℃ in trypsin solution was increased by 35.8 min comparing to the wildtype, which improved the application value of the xylanase as a feed enzyme preparation. Moreover, key amino acid residues in the catalytic pocket were identified by molecular docking, which played a crucial role in the engineering design of xylanase.

Acknowledgements

References

1. Puchart V, Uchová K, Biely P. 2021. Xylanases of glycoside hydrolase family 30 – An overview. Biotechnol Adv. 47: 107704.

2. Mahmood MS, Rasul F, Saleem M, Afroz A, Malik MF, Ashraf NM, *et al*. 2019. Characterization of recombinant endo-1,4-β-xylanase of *Bacillus halodurans* C-125 and rational identification of hot spot amino acid residues responsible for enhancing thermostability by an in-silico approach. Mol Biol Rep. 46(4):3651–3662.

3. Kumar V, Dangi AK, Shukla P. 2018. Engineering thermostable microbial xylanases toward its industrial applications. Mol Biotechnol. 60(3):226-235.

4. Pas G, Berrin JG, Beaugrand J. 2011. GH11 xylanases: structure/function/properties relationships and applications. Biotechnol Adv. 30(3):564-592.

5. Tony C, Charles G, Georges F. 2010. Xylanases, xylanase families and extremophilic xylanases. Fems Microbiol Rev. 29(1):3-23.

6. Leggio LL, Jenkins J, Harris GW, Pickersgill RW. 2000. X-ray crystallographic study of xylopentaose binding to *Pseudomonas* fluorescens xylanase A. Proteins. 41(3):362-373

7. Juturu V, Jin CW. 2012. Microbial xylanases: engineering, production and industrial applications. Biotechnol Adv. 30(6):1219-1227.

8. Bhat SK, Purushothaman K, Kini KR, Rao A. 2021. Design of mutants of GH11 xylanase from *Bacillus pumilus* for enhanced stability by amino acid substitutions in the N-terminal region: an in silico analysis. J Biomol Struct Dyn. (8):1-14.

9. Wang L, Wang Y, Chang S, Gao Z, Ma J, Wu B, *et al*. 2022. Identification and characterization of a thermostable GH11 xylanase from *Paenibacillus campinasensis* NTU-11 and the distinct roles of its carbohydrate-binding domain and linker sequence. Colloid Surface B. 209:112167.

10. Fujimoto Z, Kishine N, Teramoto K, Tsutsui S, Kaneko S. 2021. Structure-based substrate specificity analysis of GH11 xylanase from *Streptomyces olivaceoviridis* E-86. Appl Microbiol Biot. 105(5):1-10.

11. Winterhalter C, Heinrich P, Candussio A, Wich G, Liebl W. 2010. Identification of a novel cellulose-binding domain within the multidomain 120 kda xylanase xyna of the hyperthermophilic bacterium thermotoga maritima. Mol Microbiol. 15(3):431-444.

12. Chen XL, Zhao F, Yue YS, Zhang XY, Zhong Y, Yi P. 2018. Functional characterization of a new group of modular xylanases in glycoside hydrolase family 8 from marine bacteria. Appl Environ Microb. 84(23):e01785.

13. Ha DT, Kanarskiy AV, Kanarskaya ZA, Scherbakov AV, Pranovich AV. 2020. Impact of cultivation conditions on xylanase production and growth in *Paenibacillus mucilaginosus*. Proceedings of Universities Applied Chemistry and Biotechnology. 10(3):459-469.

14. Zhang C, Ding Y. 2021. Probing the relation between community evolution in dynamic residue interaction networks and xylanase thermostability. IEEE ACM T Comput Bi. 18(2):686-696.

15. Han N. 2021. Improving the thermostability of a fungal GH11 xylanase via fusion of a submodule (C2) from hyperthermophilic CBM9_1-2. Int J Mol Sci. 23:463.

16. Li G, Chen X, Zhou X, Huang R, Zhang R. 2019. Improvement of GH10 family xylanase thermostability by introducing of an extra α-helix at the C-terminal. Biochem Bioph Res Co. 515(3):417-422.

17. Yu J, Liu X, Guan L, Jiang Z, Yang S. 2020. High–level expression and enzymatic properties of a novel thermostable xylanase with high arabinoxylan degradation ability from *Chaetomium* sp. suitable for beer mashing. Int J Biol Macromol. 168:223-232.

18. Polizeli M, Rizzatti A, Monti R, Terenzi HF, Amorim DS. 2005. Xylanase from fungi: properties and industrial applications. Appl Microbiol Biotechnol. 67(5):577-591.

19. Ngo K, Silva F, Leite V, Contessoto VG, Onuchic JN. 2021. Improving the thermostability of xylanase A from *Bacillus subtilis* by combining bioinformatics and electrostatic interactions optimization. J Phy Chem B. 125(17):4359-4367.

20. Adgüzel AO. 2022. Valorization of banana pseudostem: endoxylanase production by *Streptomyces* sp. SH5027 using statistical approaches and its characterization and application in bread making. Turkish J Eng. 6(2):128-139.

21. Li C, Li J, Wang R, Li X, Wu M. 2018. Substituting both the N-terminal and "Cord" regions of a xylanase from *Aspergillus oryzae* to improve its temperature characteristics. Appl Biochem Biotech. 185(8):1-16.

22. Han N, Ma Y, Mu Y, Tang X, Huang Z. 2019. Enhancing thermal tolerance of a fungal GH11 xylanase guided by B-factor analysis and multiple sequence alignment. Enzyme Microb Tech. 131:109422.

23. Yin X, Li JF, Wang JQ, Tang CD, Wu MC. 2013. Enhanced thermostability of a mesophilic xylanase by N-terminal replacement designed by molecular dynamics simulation. J Sci Food Agr. 93(12):3016-3023.

24. Han N, Miao H, Ding J, Li J, Huang Z. 2017. Improving the thermostability of a fungal GH11 xylanase via site-directed mutagenesis guided by sequence and structural analysis. Biotechnol Biofuels. 10(133):1-12.

25. You C, Huang Q, Xue H, Yang X, Lu H. 2010. Potential hydrophobic interaction between two cysteines in interior hydrophobic region improves thermostability of a family 11 xylanase from *Neocallimastix Patriciarum*. Biotechnol Bioeng. 105(5):861-870.

26. Yang W, Yang Y, Zhang L, Hang X, Guo X, Xu Y, *et al.* 2017. Improved thermostability of an acidic xylanase from *Aspergillus sulphureus* by combined disulphide bridge introduction and proline residue substitution. Sci Rep. 7:1587.

27. Sun Z, Liu Q, Qu G, Feng Y, Reetz MT. 2019. Utility of B-factors in protein science: interpreting rigidity, flexibility, and internal motion and engineering thermostability. Chem Rev. 119(3):1626-1665.

28. Paes G, Cortés J, Siméon T, O"Donohue MJ, Tran V. 2012. Thumb-loops up for catalysis: a structure/function investigation of a functional loop movement in a GH11 xylanase. Comput Struct Biotec. 1(2):e201207001.

29. Reetz MT, Carballeira JD, Vogel A. 2010. Iterative saturation mutagenesis on the basis of B-factors as a strategy for increasing protein thermostability. Angew Chem Int Ed Engl. 118 (46):7909-7915.

30. Xue H, Zhou J, You C, Huang Q, Lu H. 2012. Amino acid substitutions in the N-terminus, cord and α-helix domains improved the thermostability of a family 11 xylanase XynR8. J Ind Microbiol. 39(9):1279-1288.

31. Cheng Z, Lan Y, Guo J, Ma D, Peplowski L. 2020. Computational design of nitrile hydratase from *Pseudonocardia thermophila* JCM3095 for improved thermostability. Molecules. 25(20):4806.

32. Nma A, Ak B, Ah A, Dk C, Amms B, Ykm, B, *et al*. 2019. Engineering of serine protease for improved thermostability and catalytic activity using rational design. Int J Biol Macromol. 126:229-237.

33. Xin L, Liu T, Zhang Y, Xin F, Sun L. 2018. Structural insights into the thermophilic adaption mechanism of Endo-1,4-β-Xylanase from *Caldicellulosiruptor owensensis*. J Agric Food Chem. 66(1):187-193.

34. Hakulinen N, Turunen O, Jänis J, Leisola M, Rouvinen J. 2003. Three-dimensional structures of thermophilic beta-1,4-xylanases from Chaetomium thermophilum and Nonomuraea flexuosa. Comparison of twelve xylanases in relation to their thermal stability. Eur J Biochem. 270(7):1399-1412.

35. Joo JC, Pack SP, Yong HK, Yoo YJ. 2011. Thermostabilization of *Bacillus circulans* xylanase: computational optimization of unstable residues based on thermal fluctuation analysis. J Biotechnol. 151(1):56-65.

36. Milos M, Jan S, Jaroslav B, Jan B, Zbynek P, Jaroslav Z, *et al*. 2017. Fireprot: web server for automated design of thermostable proteins. Nucleic Acids Res. 45:393-399.

37. Li TB, Zhu XL, Ye MY, Wang MC, Zhu JJ, Shen FJ, *et al*. 2022. Rapid improvement in thermostability of GH11 xylanase (XynASP) from *Aspergillus saccharolyticus* JOP1030-1 by tryptophan residue substitution. J Biotech Res. 13:26-39.

38. Rodrigues CHM, Pires DEV, Ascher DB. 2018. DynaMut: predicting the impact of mutations on protein conformation, flexibility and stability. Nucleic Acids Res. 46:350-355.

39. Rao SN, Head MS, Kulkarni A, Lalonde JM. 2007. Validation studies of the site-directed docking program LibDock. J Chem Inf Model. 47(6):2159-2171.

40. Konecny R, Baker NA, McCammon JA. 2012. iAPBS: a programming interface to Adaptive Poisson-Boltzmann Solver (APBS). Comput Sci Discov. 5(1):015005.

41. Liu Y, Li ZY, Guo C, Cui C, Wu ZL. 2021. Enhancing the thermal stability of ketoreductase ChKRED12 using the FireProt web server. Process Biochem. 101:207-212.

42. Pongpamorn P, Watthaisong P, Pimviriyakul P, Jaruwat A, Lawan N, Chitnumsub P. *et al*. 2019. Identification of a hotspot residue for improving the thermostability of a flavin-dependent monooxygenase. Chem Bio Chem. 20(24):3020-3031.

43. Laemmli UK. 1970. Cleavage of structural proteins during the assembly of the head of bacteriophage T4. Nature. 227(5259):680-685.

44. Wakarchuk WW, Campbell RL, Sung WL, Davoodi J, Yaguchi M. 2010. Mutational and crystallographic analyses of the active site residues of the *Bacillus circulans* xylanase. Protein Sci. 3(3):467-475.

45. Purmonen M, Valjakka J, Takkinen K, Laitinen T, Rouvinen J. 2007. Molecular dynamics studies on the thermostability of family II xylanases. Protein Eng Des Sel. 20(11):551-559.